Morphological instability of the solid-liquid interface and the supersaturation gradient in crystal growth from a high-temperature solution

Oleg A. Louchev* and Shigeki Otani
National Institute for Research in Inorganic Materials, 1-1 Namiki, Tsukuba, Ibaraki 305, Japan
(Received 13 May 1996; revised manuscript received 15 August 1996)

The problem of morphological instability is considered within the framework of linear perturbation theory for the particular case of growth of LaB_6 crystals from high-temperature solution in excess of La and B with account of the actual liquidus lines on the relevant phase diagram of Storms and Mueller, J. Phys. Chem. **82**, 51 (1978), and Otani *et al.*, J. Cryst. Growth **100**, 658 (1990). Stability is shown to be determined by the interplay of the concentration gradient, which causes instability, and the thermal effect associated with heat transfer from the solidification interface combined with the slope of the liquidus line, which inhibits instability. The thermal-kinetic effect is shown to be negligibly small for the temperature of solidification in the range 2500–2900 K. An increase in the excess of La or B solvent is shown to cause a transition from stability to instability due to (i) a sharp increase in the concentration gradient and (ii) a decrease in the temperature of the solidification interface and associated decrease in the heat transfer flux from the interface into the growing crystal, and in the derivative of the equilibrium concentration versus the solidification temperature. It is shown that the breakdown of morphological instability may take place under growth conditions without onset of increasing supersaturation in front of the solidification interface if the heat conductance of the liquid is smaller than that of the solid phase. [S1063-651X(96)12712-4]

PACS number(s): 47.20.Hw, 68.45.−v, 81.10.Dn, 81.30.−t

I. INTRODUCTION

Crystal growth from high-temperature solutions (HTS's) encompasses a broad range of techniques for producing various crystals including growth of semiconductors [1], rare-earth boride and carbide materials [2], growth of synthetic diamonds from carbon solutions in metals under high pressure and temperature [3], and so on. The crucial problem for obtaining crystals of good quality is the problem of instability of the solidification interface, which appears under certain operating conditions. The onset of instability of the growth interface leads to the appearance of a variety of microscale structures which significantly alter the various physical properties of the crystals produced, making their practical application impossible.

Instability is an intrinsic growth phenomenon associated with the nonequilibrium thermodynamic, diffusionlike processes occurring at the solidification interface. The onset of instability in HTS crystal growth is known to yield various growth structures including columnar, dendritic patterns and networks of inclusions. The problem of morphological instability for different growth modes has been treated by means of different approaches in various publications, a review of which may be found in Refs. [4] and [5]. The linear perturbation approach for atomically rough interfaces, originally developed for analyzing morphological instability in crystal growth from the melt [6], has been extended further to HTS crystal growth [7] and predicts the appearance of periodic structures in dependence on crystal growth operating conditions. Another approach [8,9] deduces the criterion for onset of instability from comparison of (i) the solute concentration gradient, which occurs due to the rejection of the solvent by propagating solidification interface, with the equilibrium concentration gradient, associated with the temperature gradient in front of the interface. Within the framework of this criterion the onset of instability takes place if the solution concentration gradient becomes higher than the equilibrium concentration gradient, yielding a supersaturation gradient (similar to constitutional supercooling in melt growth of doped crystals), which increases into the solution. This criterion indicates the existence of a thermodynamically metastable zone in front of the solidification interface within which spontaneous nucleation may occur leading to the appearance of multigrain and inclusion structures. A similar approach [10] treats the problem of morphological instability by considering the gradient of the growth velocity in the growth direction. The expression obtained, interpreted as a criterion for morphological instability, shows that the instability term associated with bulk diffusion is enhanced by the thermally activated kinetics, and is inhibited by the gradient of the equilibrium concentration.

Our present study is motivated by ongoing experimental research in the field of HTS growth, including the growth of semiconductor crystals [1] by the traveling heater method and boride crystals by the float-zone traveling solvent technique [11–13]. These studies aim to reveal the hidden mechanisms, underlying the formation of the various types of defects occurring in these crystals under different growth conditions, i.e., growth rate, temperature of solidification, and temperature gradient across the interface. The results obtained reveal that the thermal phenomena strongly influence growth pattern formation. In the present paper we refocus on the problem of morphological instability in HTS crys-

*Electronic address: loutchev@nirim.go.jp

tal growth for the particular case of LaB_6 growth from solutions with an excess of La or B. Our procedure combines (i) a linear perturbation approach, accounting for the dependence of interface free energy on the perturbation wavelength, (ii) thermally activated incorporation kinetics, and (iii) the transport phenomena model, which includes diffusion mass transport, equilibrium concentration of solute and temperature gradients at both sides of the solidification interface.

The article is structured as follows. In Sec. II we present a model of high-temperature solution growth which takes into account the relevant phase diagram, growth kinetics, and heat and mass fluxes on the growth interface. In Sec. III we perform a linear stability analysis, yielding the relevant dispersion equations. In Sec. IV we consider a particular case of solidification of LaB_6 crystals from high-temperature solution in excess of La or B. In Sec. IV A we present a one-dimensional (1D) approximation which allows us to treat the problem easily and in Sec. IV B we give the main results. Finally, in Sec. V we give an outline of the main conclusions drawn from our study.

II. MODEL

Let us consider a macroscopically planar area of the atomically rough solidification interface moving with a growth rate V under the diffusion flux of solute and conductive heat flux through the interface. We assume that the characteristic wavelength of ''stable'' perturbations $\lambda_{\max}$ occurring under ''unstable'' conditions is considerably smaller than the characteristic linear dimension of this area. This allows us to treat the macroscopic ''unperturbed'' parameters relevant to the problem as uniform within this area. We assume also that the distributions of all macroscopic unperturbed parameters are known from 2D numerical simulations models [14] or 1D analytical approximation [15] providing us with the values of growth rate V, concentration at the interface C_i, temperature of interface T_i, and the gradients of (i) concentration $G_c=\mathbf{n}\mathrm{grad}C$ and (ii) temperature gradients from both sides of the interface: $G_{T_s}=\mathbf{n}\ \mathrm{grad}\ T_s$ and $G_{T_1}=\mathbf{n}\ \mathrm{grad}\ T_1$. We consider the problem in the frame of reference attached to the interface with the one x axis directed into the solution and the y axis along the interface. The mass transport equation for the solute we consider within the boundary layer neglecting all convective terms in comparison with diffusion except the component of velocity normal to the growth interface associated with growth rate V and corresponding $x0y$ frame movement. In the heat transfer equation, we neglect all convective terms, assuming that they are small in comparison with heat conduction. In our model we neglect also the anisotropy of growth, surface diffusion, and also fluid motion induced by a density difference of solid and liquid phases.

Let us disturb the planar solidification interface by a perturbation in the form of a normal mode:

$$h(y)=h^*\exp(\omega t+iay), \tag{1}$$

where h^* is the amplitude, and ω and $a=2\pi/\lambda$ are its increment and wave number, respectively. Let us consider the growth velocity V in the following linear form [16]:

$$V|_{x=h(y)}=\Omega\beta(T_i)\{C|_{x=h(y)}-C_{\mathrm{eq}}(T_i)\}, \tag{2}$$

where Ω is the volume per one molecule (atom) in solid, C_i is the concentration of the solute in front of the interface, T_i is the interface temperature and $C_{\mathrm{eq}}(T_i)$ is the equilibrium concentration of the curved interface given in accordance with the Gibbs-Thompson effect as

$$C_{\mathrm{eq}}(T_i)=C^0_{\mathrm{eq}}(T_i)-\frac{C^0_{\mathrm{eq}}(T_i)\Omega\gamma}{k_BT_i}\frac{h''_{yy}}{[1+(h'_y)^2]^{3/2}}, \tag{3}$$

where C^0_{eq} is the equilibrium concentration of a flat interface, γ is the interfacial free energy, and k_B is the Boltzmann constant. The kinetic coefficient in Eq. (2) is expressed as [16]

$$\beta(T_i)\cong\frac{\nu a_0^2}{\lambda_k}\exp\left(-\frac{\Delta E_a}{k_BT_i}\right), \tag{4}$$

where a_0 is the interatomic distance, λ_k is the average distance between the kinks, ΔE_a is the activation energy, and $\nu\cong10^{13}$ Hz is the thermal vibration frequency.

The concentration within the diffusion boundary layer is governed by

$$\frac{\partial C}{\partial t}-V\frac{\rho_s}{\rho_1}\frac{\partial C}{\partial x}=D_1\left(\frac{\partial^2C}{\partial x^2}+\frac{\partial^2C}{\partial y^2}\right), \tag{5}$$

where ρ_s/ρ_l is the ratio of density of solid to liquid phases and D_1 is the diffusion coefficient.

The boundary condition on the interface $x=h(y)$ reflects the balance between (i) the convective-diffusion flux from solution and (ii) liquid-solid phase interchange as follows:

$$V\frac{\rho_s}{\rho_1}C+D_1\left(\frac{\partial C}{\partial x}-\frac{\partial C}{\partial y}\frac{\partial h}{\partial y}\right)=\beta(T_i)\{C-C_{\mathrm{eq}}(T_i)\}. \tag{6}$$

Assuming that the perturbation zone in the solute is smaller than the diffusion boundary layer we formulate the second boundary condition as

$$\left.\frac{\partial C}{\partial x}\right|_{x\to\infty}=G_C. \tag{7}$$

The heat transfer through the growth interface is governed by two equations:

$$\frac{\partial T_1}{\partial t}=a_1\left(\frac{\partial^2T_1}{\partial x^2}+\frac{\partial^2T_1}{\partial y^2}\right), \tag{8}$$

$$\frac{\partial T_s}{\partial t}=a_s\left(\frac{\partial^2T_s}{\partial x^2}+\frac{\partial^2T_s}{\partial y^2}\right), \tag{9}$$

for the liquid $x>h(y)$ and solid $x<h(y)$ phases, where a_1 and a_s are the thermal diffusivities for liquid and solid phases, respectively. The boundary conditions are given by the following set of equations:

$$\left.\frac{\partial T_1}{\partial x}\right|_{x\to\infty}=G_{T_l}. \tag{10}$$

$$\left.\frac{\partial T_s}{\partial x}\right|_{x\to-\infty}=G_{T_s}. \tag{11}$$

$$T_1|_{x=h(y)}=T_s|_{x=h(y)}=T_i, \tag{12}$$

where the values of G_{T_s} and G_{T_l} correspond to the temperature gradients at the nonperturbed flat interface. Besides the boundary condition we consider the heat balance at the interface $x=h(y)$:

$$k_s\left(\frac{\partial T_s}{\partial x}-\frac{\partial T_s}{\partial y}\frac{\partial h}{\partial y}\right)=k_1\left(\frac{\partial T_1}{\partial x}-\frac{\partial T_1}{\partial y}\frac{\partial h}{\partial y}\right)+\rho_s\Delta HV, \tag{13}$$

where k_s and k_1 are the heat conductances of solid and liquid phases, respectively.

III. LINEAR PERTURBATION ANALYSIS

To treat the above problem by the linear perturbation technique, we linearly expand the values of (i) the equilibrium concentration $C_{\rm eq}(T_i)$ and (ii) the kinetic coefficient $\beta(T_i)$ near the base state interface temperature T_i. Analyzing the response of all quantities governed by the above model to solidification interface perturbation, given by Eq. (1), we finally find the dispersion equation:

$$\varpi=\frac{G_C+(\eta\Delta C_0-\alpha)G_T\left(1+\frac{\rho_s}{\rho_1}\frac{V}{D_1\zeta_1}\right)-\frac{C^0_{\rm eq}(T_i)\Omega\gamma}{k_BT_i}a^2\left(1+\frac{\rho_s}{\rho_1}\frac{V}{D_1\zeta_1}\right)}{\frac{\beta(T_i)-D_1\zeta_1}{\Omega\beta(T_i)D_1\zeta_1}-\frac{\rho_s}{\rho_1}\left(\frac{G_C}{D_1(a^2+\varpi/D_1)}-\frac{C_i}{D_1\zeta_1}\right)-\frac{(\eta\Delta C_0-\alpha)\rho_s\Delta H}{k_1\zeta_2+k_s\zeta_3}}, \tag{14}$$

where $\zeta_1=-1/2(\rho_s/\rho_1)V/D_1-\sqrt{1/4[(\rho_s/\rho_1V/D_1)]^2+a^2+\varpi/D_1}$, $\zeta_2=\sqrt{a^2+\varpi/a_1}$ and $\zeta_3=\sqrt{a^2+\varpi/a_s}$.

In Eq. (14) the value of

$$G_T=\frac{k_1\zeta_2G_{T_1}+k_s\zeta_3G_{T_s}}{k_1\zeta_2+k_s\zeta_3} \tag{15}$$

represents the average temperature gradient at the interface and the values of η and α are given by

$$\eta=\frac{1}{\beta(T_i)}\left.\frac{d\beta}{dT}\right|_{T_i}=\frac{\Delta E_a}{k_BT_i^2}, \tag{16}$$

$$\alpha=\left.\frac{dC^0_{\rm eq}}{dT}\right|_{T_i}. \tag{17}$$

In the case when the characteristic times of the diffusion and heat diffusion equations associated with the applied perturbation are negligibly small, i.e., $(D_1a^2)^{-1}$, $(a_1a^2)^{-1}$, $(a_sa^2)^{-1}\ll|\varpi|^{-1}$, we obtain an explicit dependence of the perturbation increment ϖ, on the perturbation wave number a:

$$\varpi=\frac{\Omega D_1a\left\{G_C+(\eta\Delta C_0-\alpha)G_T\left(1-\frac{\rho_s}{\rho_1}\frac{V}{D_1a}\right)-\frac{C^0_{\rm eq}(T_i)\Omega\gamma}{k_BT_i}a^2\left(1-\frac{\rho_s}{\rho_1}\frac{V}{D_1a}\right)\right\}}{\frac{\beta(T_i)+D_1a}{\beta(T_i)}-\frac{\rho_s\Omega}{\rho_1}\left(\frac{G_C}{a}+C_i\right)-\frac{\Omega D_1(\eta\Delta C_0-\alpha)\rho_s\Delta H}{(k_1+k_s)}}, \tag{14'}$$

where

$$G_T=\frac{k_1G_{T_1}+k_sG_{T_s}}{k_1+k_s} \tag{15'}$$

is the average temperature gradient across the interface.

The dispersion expressions (14) and (15) show that the morphological stability of the growth interface is determined by three interfering effects (the estimates show that the denominator of Eqs. (14) is positive for operating conditions of solidification from solutions). First, the bulk diffusion term, represented by G_C, corresponds to an enhancement of the growth rate on the tip of the perturbation due to an increase in the concentration C_i being the main cause of the morphological instability. Second, a thermal-kinetic term, represented by $\eta\Delta C_0G_T$, corresponds to the enhancement of the growth rate on the tip of the perturbation due to an increase in the temperature T_i and an associated increase in the kinetic coefficient $\beta(T_i)$. This effect enhances the instability for the mode when the average temperature gradient is positive. This is true provided that temperature supercooling does not take place in the liquid phase in front of the growth interface. Third, a thermal term, represented by αG_T, corresponds to a decrease of the growth rate on the tip of the

perturbation due to an increase in the equilibrium concentration C_{eq} caused by the temperature increase. This effect inhibits the morphological instability caused by the two previously mentioned effects for the case of positive average temperature gradient, G_T. In the case of the onset the temperature supercooling in the liquid phase in front of the solidification interface which, for instance, may appear in float-zone crystal growth under high pulling rates [17] the average temperature gradient may become negative. In this mode the thermal term αG_T will enhance the instability along with the diffusion term G_C, while the thermal-kinetic term $\eta\Delta\, C_0 G_T$ will inhibit the instability. Equation (14) gives the following criterion for the morphological instability of the solidification interface in crystal growth from solution [18]:

$$G = G_C + (\eta\Delta C_0 - \alpha) G_T > 0. \tag{18}$$

This criterion means that if the value of the generalized gradient G is positive then the diffusion enhanced by the thermal-kinetic instability is no longer compensated for by the thermal effect associated with the liquidus line slope on the phase diagram and average temperature gradient. This criterion differs from that of increasing supersaturation gradient [4], which may be written as

$$G^* = G_C - \alpha G_{T_1} > 0. \tag{19}$$

This criterion takes into account the temperature gradient in the liquid phase $G_{T_1} = \mathbf{n}\ \mathrm{grad}\ T_1$ while the thermal perturbation of the solidification interface depends on the temperature gradients in both phases [Eq. (14)], similar to the case of interface perturbation in crystal growth from supercooled melts [6]. Criterion (18) agrees well with the criterion obtained by the growth velocity gradient approach [6,10] and gives a more accurate treatment of the contribution of the relevant thermal effects. As will be shown later, this may lead to a considerable difference between criteria in the particular case of HTS growth of LaB_6 crystals and is crucial for understanding the origins of occurring microscale defect patterns.

IV. MORPHOLOGICAL INSTABILITY AND SUPERSATURATION GRADIENT

A. HTS growth of LaB_6

In order to be more specific we will now consider the problem of morphological instability for the particular case of HTS growth of LaB_6 crystals in excess of (i) La and (ii) B. Crystals of LaB_6 are currently used as electron emitters of high brightness and longevity [2] and their growth in excess of La [11,12] or B [13] allows crystals of better quality than those from the conventional float-zone technique to be obtained. The excess of La or B, provided initially within the processed specimen, allows the temperature of dissolution and solidification to be decreased in accordance with the phase diagram shown in Fig. 1. The dashed lines in this figure show the data obtained by Storms and Mueller [19] while solid lines represent data obtained by Otani *et al.* [20] that exhibit a considerably weaker dependence of the solid-liquid transition temperature on the value of B:La atomic ratio r.

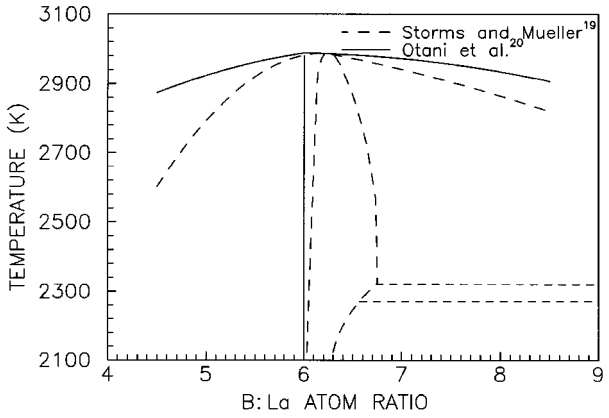

FIG. 1. Part of the La-B phase diagram by Storms and Mueller (Ref. [19]) and Otani *et al.* (Ref. [20]).

We note here that the thermal-kinetic term $\eta\Delta C_0 G_T$ may markedly contribute to the instability when the temperature of solidification is below $\cong$1500 K. However, a thermal analysis of the float-zone traveling solvent growth of LaB_6 carried out in Ref. [15] shows that the characteristic range of the solidification temperature is 2500–2900 K and the effect of the kinetic resistance is negligibly small. Thus, the growth rate is determined by the interplay of quasi-steady-state heat and mass transfer from the dissolution to the solidification interface. Therefore, neglecting non-steady-state effects, and for negligibly small kinetic resistance setting (i) $\Delta C_0 \to 0$, (ii) $C_i \to C^0_{eq}(T_i)$, and (iii) $[\beta(T_i) + D_1 a]/\beta(T_i) \to 1$, we obtain the following dispersion equation for this particular case:

$$\varpi = \frac{\Omega D_1 a \left\{ G_C - \alpha G_T - \dfrac{C^0_{eq}(T_i)\Omega\gamma}{k_B T_i}\, a^2 \right\}}{1 - \dfrac{\rho_s \Omega}{\rho_1}\left(\dfrac{G_C}{a} + C^0_{eq}(T_i) \right) + \dfrac{\Omega D_1 \alpha \rho_s \Delta H}{(k_1 + k_s)}}. \tag{20}$$

Without the thermal-kinetic effect, when $\eta = 0$, the stability condition is essentially that of Mullins and Sekerka [6] deduced for the case of crystal growth from the melt when the impurities or dopants rejected by the progressing solidification interface decrease the equilibrium temperature of solid-liquid transition. However, it is worth noting that in high-temperature solutions and, for instance, in traveling solvent crystal growth, the temperature of solidification is not fixed and depends on many operational parameters. As will be shown later the possible shift of the temperature of solidification within the range 2500–2900 K may alter strongly the concentration gradient G_c [see Eq. (24) below] responsible for the instability as well as the term αG_T responsible for stabilization of the growth interface.

The maximum of the increment under the instability condition, $G = G_C - \alpha G_T > 0$ corresponds to the perturbation wavelength given by [21]

$$\lambda_{max} \cong 2\pi \left[\frac{3}{G_C - \alpha G_T} \frac{C^0_{eq}(T_i)\Omega\gamma}{k_B T_i} \right]^{1/2}. \tag{21}$$

To obtain numeric estimates we consider the growth of LaB_6 crystal in the simplified form of a semi-infinite cylindrical rod in the 1D heat transfer approximation neglecting

the radial component of the heat conductance equation [22] and assuming that the heat transport by specimen movement is negligible in comparison with axial heat conduction [23]. Under the above assumptions the value of the temperature gradient inside the solid phase in the 1D approximation including radiative and convective heat removal from the lateral surface may be expressed as [24]

$$G_{T_s}=\left\{\frac{4k_s}{R}\left[0.5h_c(T_i^2-T_0^2)-h_cT_0(T_i-T_0)\right.\right.$$
$$\left.\left.+0.2\varepsilon\sigma(T_i^5-T_0^5)-\varepsilon\sigma T_0^4(T_i-T_0)\right]\right\}^{1/2}, \quad (22)$$

where R is the crystal radius, $h_c\cong 30$ W/m^2 K is the convective heat transfer coefficient, $\varepsilon\cong 0.7$ is the crystal emissivity, σ is the Stefan-Boltzman constant and $T_0=300$ K is the ambient temperature of heat removal from the lateral surface of the crystal. This expression allows us to obtain the value of the average temperature gradient via the heat balance on the growth interface as

$$G_T=\frac{2k_sG_{T_s}-\rho_s\Delta HV}{k_s+k_1}\cong\frac{2k_sG_{T_s}}{k_s+k_1}. \quad (23)$$

In steady-state growth mode the crystal growth rate is adjusted to the operational pulling rate at which the crystal is pulled out from the solution. This allows us to express the value of the concentration gradient G_C through the value of the pulling rate as

$$G_C=\frac{V}{\Omega D_1}-\frac{\rho_s}{\rho_1}\frac{VC^0_{\rm eq}(T_i)}{D_1}. \quad (24)$$

We will consider here the stability of the solidification interface for two cases, corresponding to the growth from solution with excess of La ($4<r<6$) and to the growth from solution in excess of B ($6<r<8$). For the case of La excess we assume that the solidification is controlled by the mass transfer of B, the equilibrium concentration of which is expressed through the solution density as

$$C^0_{\rm eqB}(T_i)=\frac{r\rho_{\rm sol}}{rM_{\rm B}+M_{\rm La}}, \quad (25)$$

and the value of α is given as [25]

$$\alpha=\left.\frac{dC^0_{\rm eq}}{dT}\right|_{T_i}\cong\frac{M_{\rm La}\rho_{\rm sol}}{(rM_{\rm B}+M_{\rm La})^2}\left.\frac{dr}{dT}\right|_{T_i}, \quad (26)$$

where $M_{\rm B}$ and $M_{\rm La}$ are the atomic masses of B and La, respectively, and $r(T_i)$ corresponds to the liquidus line on the phase diagram. For the case of B excess we assume that the solidification is controlled by the mass transfer of La, the equilibrium concentration of which is expressed through the solution density as

$$C^0_{\rm eqLa}(T_i)=\frac{\rho_{\rm sol}}{rM_{\rm B}+M_{\rm La}}, \quad (25')$$

and the value of α is given as [25]

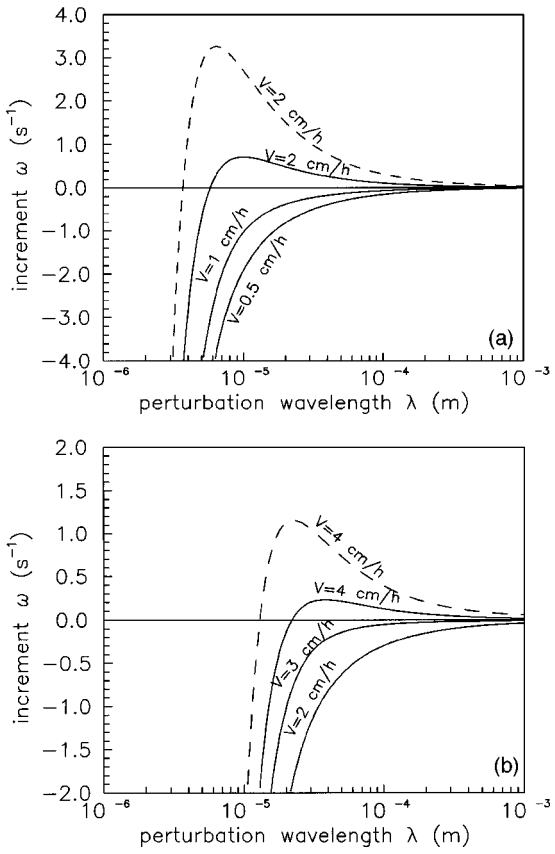

FIG. 2. The dependence of the perturbation increment versus the perturbation wavelength for various growth rates of LaB_6 in excess of La (a) and B (b), calculated for the Otani *et al.* (Ref. [20]) phase diagram (solid lines) and Storms and Mueller (Ref. [19]) phase diagram (dashed lines).

$$\alpha=\left.\frac{dC^0_{\rm eq}}{dT}\right|_{T_i}\cong-\frac{M_{\rm B}\rho_{\rm sol}}{(rM_{\rm B}+M_{\rm La})^2}\left.\frac{dr}{dT}\right|_{T_i}. \quad (26')$$

In our calculations we have used the following set of physical data: $\Omega_{\rm B}=1.18\times10^{-29}$ m^3, $\Omega_{\rm La}=7.08\times10^{-29}$ m^3, $k_s=k_1\cong 30$ W/mK, $\rho_{so}\cong\rho_s\cong 4760$ kg/m^3, $D_1\cong 5\times10^{-9}$ m^2/s, and $\Delta H\cong10^6$ J/kg. The value of interfacial free energy for the cubic crystal lattice is estimated to an order of magnitude as $\gamma\cong\Delta H'/6a_0^2\cong 330$ mJ/m^2, where $\Delta H'=3.37\times10^{-19}$ J is the latent heat per one molecule of LaB_6 and $a_0=4.1$ Å is the lattice parameter. All calculations are carried out for a crystal radius $R=5$ mm.

B. Results and discussion

In Figs. 2(a) and 2(b) we present the dependence of the perturbation increment, ϖ on the perturbation wavelength for various pulling rates for the case of growth in (a) excess of La, $r=4$, and (b) excess of B, $r=8$. The solid curves correspond to the phase diagram of Otani *et al.* [20] while the dashed curves correspond to that of Storms and Mueller [19]. Solid curves in Fig. 2(a) show that for pulling rates $V=0.5$ and 1 cm/h the value of ϖ does not become positive with increase of perturbation wavelength and, therefore, the solidification interface is stable. Only for the growth rate

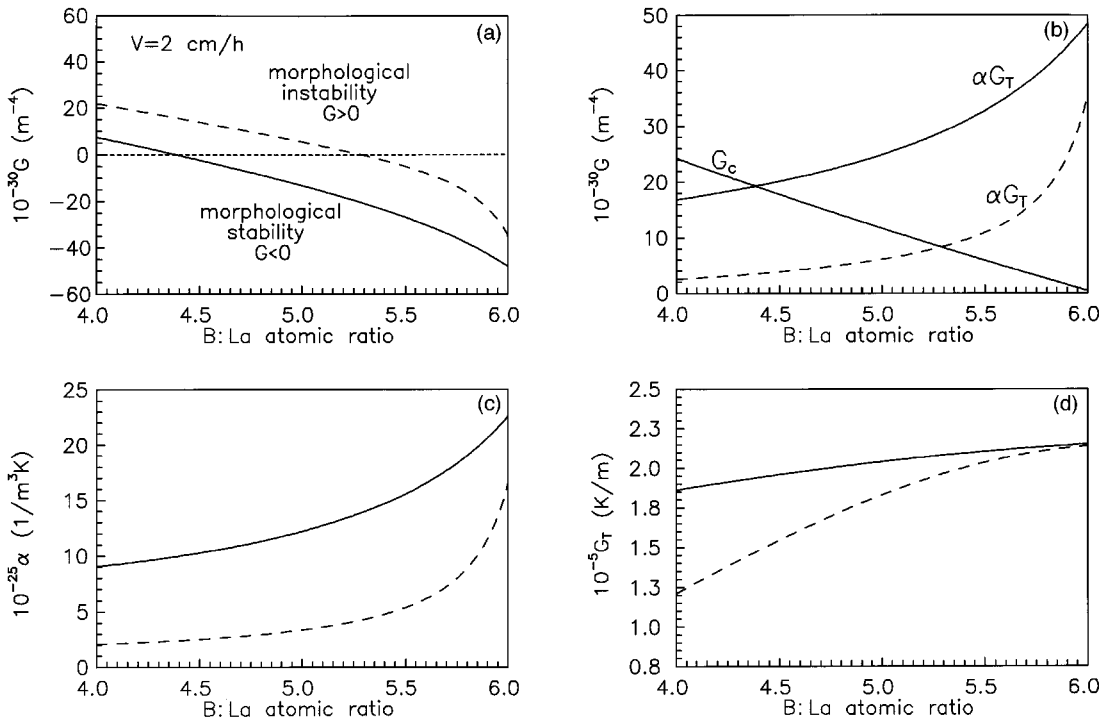

FIG. 3. The dependence of generalized gradient, calculated for Otani *et al.* (Ref. [20]) (solid) and Storms and Mueller (Ref. [19]) (dashed) data, exhibits a transition from instability ($G>0$) to stability ($G<0$) with increase of B:La ratio from $r=4$ to $r=6$ for the given growth rate (a). An increase in the B:La ratio leads to a decrease in the concentration gradient G_C (a) and increase in the thermal inhibition term αG_T (b) due to increase in $\alpha=dC^0_{\rm eq}/dT_i$ (c) and average temperature gradient G_T (d).

$V=2$ cm/h is the value of ϖ found to become positive for $\lambda=\lambda_0>5$ μm and to have maximum at $\lambda_{\max}\cong 9$ μm. In the case of the Storms and Mueller liquidus line, λ_0 and $\lambda_{\max}$ shift to smaller values due to the smaller values of $|dr/dT|$ on the liquidus line. For the case of growth in excess of B, a shift to the better interface stability occurs due to the larger values of $|dr/dT|$ for $r>6$ in comparison with excess of La, $r<6$. For the case considered, $r=8$, the interface stability is ensured for $V=3$ cm/h.

In Fig. 3(a) we present the dependence of the generalized gradient, $G=G_C-\alpha G_T$, versus the B:La atomic ratio within the range $4<r<6$ for the given pulling rate $V=2$ cm/h for the two sets of the liquidus line data. The increase of La content reveals the transitions from interface instability $G>0$ to stability $G<0$. The case of the Otani *et al.* [20] diagram corresponds to the larger stability range, $r>4.4$, in comparison with that of Storms and Mueller, $r>5.3$. The details explaining these dependencies are given in Figs. 3(b)–3(d). In Fig. 3(b) we present the corresponding dependence of the instability driving diffusion gradient, G_C, together with the thermal term, αG_T, which inhibits this instability. The curves are given for both sets of the liquidus line data considered. The concentration gradient is shown to decrease sharply when the value of r approaches the stoichiometric point ($r=6$) since the value of $\rho_s C^0_{\rm eq}(T_i)/\rho_1$ tends towards Ω^{-1} and therefore $G_C\to 0$. However, the value of αG_T increases with increase in r. This is due to the combined action of two effects. First, the increase of r leads to an increase in T_i and to an increase in $\alpha\propto dr/dT_i$, shown in Fig. 3(c). Second, the increase of r leading to the increase in T_i also increases the heat transfer flux from the solidification interface into the growing crystal and, thereby, the value of the average temperature gradient at the solidification interface, as shown in Fig. 3(d). The intersection of G_C with αG_T gives the transition from instability to stability. Figures 3(c) and 3(d) show that the liquidus line of Otani *et al.* [20] which has larger values of T_i and dr/dT_i with larger values of α and G_T implies a considerably larger range of stability in comparison with that of Ref. [19].

In Figs. 4(a) and 4(b) we show the dependence of the generalized gradient G on the growth rate (a) and the wavelength $\lambda_{\max}$ corresponding to the maximum of increment (b), both calculated for various values of the B:La atomic ratio for the case of Otani *et al.* [20] data. Solid lines in Fig. 4(b) correspond to the present model and the dashed line is calculated taking into account only the effect of the diffusion driven instability and neglecting the thermal inhibition term. Figure 4 a shows that the increase of V leads to the transition from stability ($G<0$) to instability ($G>0$) at the definite threshold rate. An increase of the B:La ratio ($4<r<6$) shifts this transition to larger threshold values of the growth rate. At these threshold growth rates the value of $\lambda_{\max}$ tends towards infinity (since $G\to 0$). The value of $\lambda_{\max}$ is shown to decrease very sharply from the level of several hundreds of microns down to $\cong 10$ μm. For instance, for $r=4$ this decrease occurs within the growth range from $\cong 1.4$ to 2 cm/h. The growth in excess of B shown reveals the same qualitative behavior, with a shift of the instability-stability transition threshold to larger values of the growth rate when the B:La atomic ratio approaches the stoichiometry point $r=6$. The maximum of increment is shifted for this case to larger values of $\lambda_{\max}$ ranging from several hundreds of microns to a

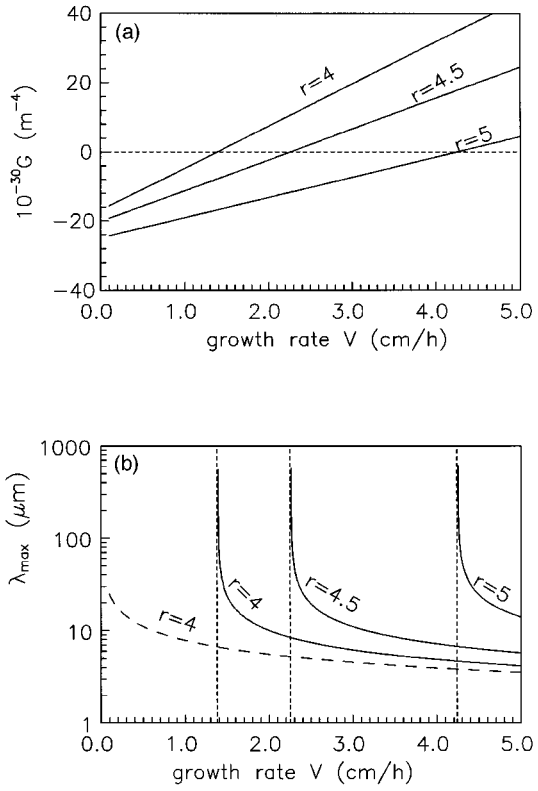

FIG. 4. An increase in the growth rate leads to a transition from stability ($G<0$) to instability ($G>0$) (a) yielding the appearance of growth structures of critical wavelength λ_{max} (solid lines) (b) for the growth rates higher than a certain threshold value corresponding to the given B:La ratio (<6, excess of La) while the diffusion model (dashed line) yields a continuous dependence of λ_{max} versus V, ranging from $\cong$20 to $\cong$10 μm. An increase in r leads to an extended range of stability.

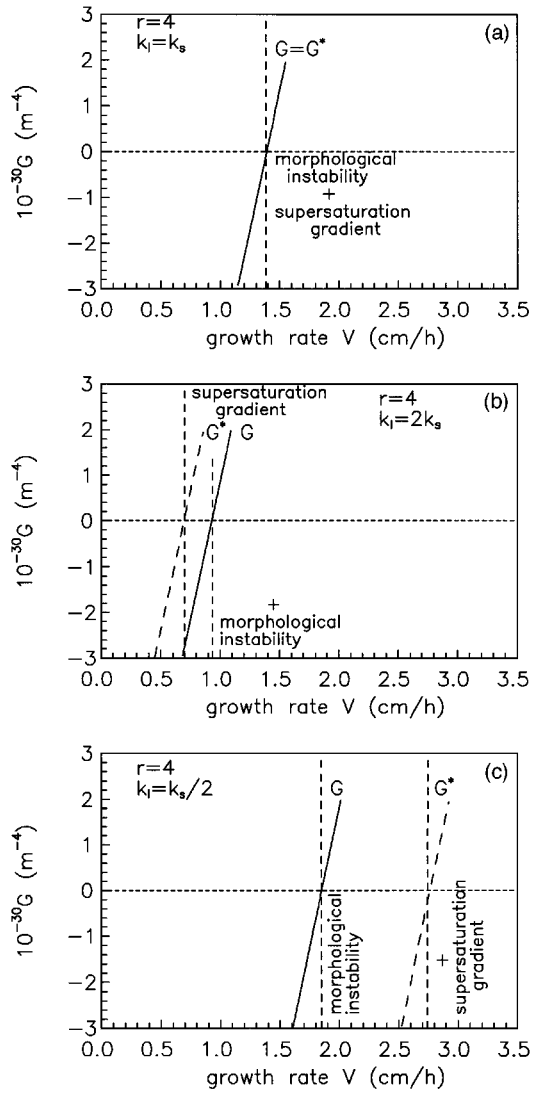

FIG. 5. The dependencies of G and G^* on increase in the growth rate show (a) the simultaneous onset of morphological instability and increasing supersaturation gradient for $k_l=k_s$, (b) the onset of increasing supersaturation gradient before the onset of morphological instability for $k_l>k_s$, and (c) the onset of morphological instability before the onset of increasing supersaturation gradient for $k_l<k_s$.

few tens of microns. The graphs for λ_{max} shown in Fig. 4(b) reveal that the preferential perturbation wavelength may attain the length of several hundreds of microns if the growth rate is held close enough to the threshold value.

Let us now consider the criterion for the onset of the supersaturation gradient (constitutional supercooling) in front of the solidification interface. For the case of the diffusion controlled growth of LaB_6 with $C_i \rightarrow C^0_{eq}(T_i)$ the onset of increasing supersaturation gradient takes place when the slope of the concentration gradient G_C becomes larger than that of the slope of the equilibrium concentration, corresponding to the temperature slope of the liquid phase in front of the solidification interface αG_{T_l}. Thus, the criterion for the onset of the supersaturation gradient, expression (19), differs from that of onset of morphological instability, given by expression (18), where the value of the average temperature gradient is used.

In all the above calculations we have used the same values of the heat conductance, $k_s=k_1\cong 30$ W/m K for both phases and the value of the latent heat release is negligibly small so that $G_{T_l}=G_T=G_{T_s}$ and the curve for the criterion of the morphological stability G coincides with that of criterion for the onset of the supersaturation gradient G^*. However, the heat conductances of solid and liquid phases may considerably differ and thus these criteria will contrast markedly with each other. Unfortunately, there is a lack of data on the behavior of the heat conductance of LaB_6. The possible difference of heat conductance of solid and liquid phases may lead to different curves for the morphological instability criterion and the criterion for the onset of the supersaturation gradient. In Figs. 5(a)–5(c) we show the behavior of G and G^* for the cases of (a) $k_s=k_1\cong 30$ W/m K, (b) $k_1\cong 2k_s=60$ W/m K, and (c) $k_1\cong 0.5k_s=15$ W/m K. The case of the equal heat conductances gives coinciding curves for G and G^*, as shown in Fig. 5(a). In the case shown in Fig. 5(b) the larger value of liquid heat conductance leads to the onset of the supersaturation gradient at a markedly smaller growth rate, $V\cong 0.7$ cm/h, than that for the onset of morphological instability, $V\cong 0.9$ cm/h. This is due to the difference in G_{T_l}

$=G_{T_s}/2$ and $G_T=2G_{T_s}/3$. In the case shown in Fig. 5(c) the smaller value of liquid heat conductance yields an onset of the supersaturation gradient at markedly larger growth rate, $V\cong 2.75$ cm/h, than that for the onset of morphological instability, $V\cong 1.85$ cm/h. This is due to the difference in $G_{T_l}=2G_{T_s}$ and $G_T=4G_{T_s}/3$.

Let us now discuss how the effects considered above may reveal themselves experimentally. The onset of morphological instability should lead to the appearance of interface waviness, which is known to be the precursor of growth of the columnar structures. The onset of the supersaturation gradient leads to the occurrence of a metastable supersaturated solution zone in front of the solidification interface. If this supersaturation reaches the critical value homogeneous nucleation occurs within the region with the supersaturation above critical. If the supersaturation gradient occurs at smaller growth rates than the morphological instability ($k_1>k_s$), morphological instability has not yet occurred, and if the supersaturation within the supersaturated area reaches the critical value then the solidification interface will be kept planar and the nuclei will appear in front of and attach to it. Inasmuch as the solidification front is stable, the attached nuclei should decrease the local growth rate and, thus, they will finally be trapped by the progressing LaB_6 solidification interface. The coalescence of these nuclei with the progressing solidification interface may also cause solute trapping leading thereby to the appearance of inclusions in crystals produced. The composition of these inclusions should differ from the stoichiometric composition. That is, for growth in excess of La with $r\cong 4$ the composition of these inclusions will be close to LaB_4. Under higher growth rates, when the onset of morphological instability takes place these nuclei, being a local perturbation, will lead to an increase in the local growth rate leading thus to the appearance of columnar and dendritic structures. If morphological instability occurs at smaller growth rates than the constitutional supercooling ($k_1<k_s$) and the supersaturation gradient has not yet occurred then the solidification interface should become wavy giving rise to growth of the columnar and dendrititic structures. The appearance of growth columns and dendrite branches may also cause solute trapping and associated inclusions in crystals. The increase of the growth rate beyond the threshold value for the onset of supersaturation gradient will lead to the occurrence within the supersaturated area of nuclei that will be trapped by the unstable solidification interface leading to dendritic structures with inclusions of smaller B content in the case of growth in excess of La.

V. CONCLUSIONS

In this study we have considered the problem of the morphological instability of an atomically rough interface in LaB_6 crystal growth from high-temperature solutions within the framework of linear perturbation theory including diffusion mass transfer, heat transfer through the growth interface, incorporation kinetics, relevant phase diagram, and interfacial free energy.

We have found that for the case of positive average temperature gradient (no temperature supercooling) the solute concentration driven instability may be enhanced by the thermally activated kinetics and is inhibited by the thermal effect associated with the slope of the liquidus line on the relevant phase diagram. In the particular case of LaB_6 growth from high-temperature solution in excess of La or B the stability of the solidification interface is shown to be determined by the interplay of the concentration gradient, which causes instability, and the thermal effect associated with heat transfer from the solidification interface combined with the slope of liquidus line, which inhibits instability. The thermal/kinetic effect is shown to be negligibly small for a temperature of solidification in the range 2500–2900 K. The competition of these two effects determines the transition from stability to instability. An increase in the excess of La or B solvent is shown to cause a transition from stability to instability due to (i) a sharp increase in the concentration gradient and (ii) a decrease in the temperature of the solidification interface and associated decrease in the heat transfer flux from the interface into the growing crystal, and (iii) a decrease in the derivative of the equilibrium concentration versus the solidification temperature. The increase of the growth rate is shown to lead to transition from stability to instability due to an increase in the concentration gradient in front of the solidification interface.

We have compared the criterion of morphological instability of the growth interface with that for the onset of supersaturation gradient in front of the interface. These two criteria are shown to be equal only for the particular case of equal heat conductances of solid and liquid phases (and when the latent heat is negligibly small in comparison with conductive heat transfer). If the heat conductance of liquid is larger than that of the solid then the onset of the supersaturation gradient occurs at smaller growth rates than the onset of the morphological instability of the solidification interface. If the supersaturation reaches the level of the homogeneous nucleation this will lead to the appearance of nuclei which will then coalesce with the progressing solidification interface. This may lead to solvent trapping causing thereby the appearance of inclusions with a higher content of solvent material. In this case the inclusions will appear at smaller growth rates than those at which the interface waviness and columnar and dendrite structures appear. If the heat conductance of the solid is larger than that of the liquid then the onset of morphological instability occurs at smaller growth rates than the onset of supersaturation gradient. In this case the waviness and columnar structures will appear at smaller growth rates than the appearance of nuclei in front of the growth interface.

ACKNOWLEDGMENTS

We would like to express our gratitude to Dr. J. Hester (NIRIM) for reading the manuscript and providing useful suggestions. One of the authors (O.A.L.) would like to express his gratitude to The Science and Technology Agency of Japan for financial support.

[1] R. Schwarz and K. W. Benz, J. Cryst. Growth **144**, 150 (1994), and references therein.
[2] S. Otani and Y. Ishizawa, Prog. Cryst. Growth Charact. **23**, 153 (1991).
[3] H. Kanda and T. Sekina, in *Properties and Growth of Diamond*, edited by G. Davies (INSPEC, London, 1994), pp. 403–415, and references therein.
[4] D. Elwell and H. J. Scheel, *Crystal Growth from High Temperature Solutions* (Academic, London, 1975).
[5] A. A. Chernov and T. Nishinaga, in *Morphology of Crystals, Part A*, edited by I. Sunagawa (Terra, Tokyo, 1987).
[6] W. W. Mullins and R. F. Sekerka, J. Appl. Phys. **35**, 444 (1964), and recent review by S. R. Coriell and G. B. McFadden, in *Handbook of Crystal Growth, V.1b*, edited by D. T. J. Hurle (Elsevier, Amsterdam, 1993).
[7] P. G. Shewmon, Trans. AIME **233**, 736 (1965).
[8] D. Elwell and B. W. Neate, J. Mater. Sci. **6**, 1499 (1971).
[9] H. J. Scheel and D. Elwell, J. Electrochem. Soc. **120**, 818 (1973).
[10] J. C. Brice, J. Cryst. Growth **6**, 9 (1969).
[11] S. Otani and Y. Ishizawa, J. Cryst. Growth **118**, 461 (1992).
[12] S. Otani, S. Honma, and Y. Ishizawa, J. Alloys Compd. **193**, 286 (1993).
[13] S. Otani, S. Honma, Y. Yajima, and Y. Ishizawa, J. Cryst. Growth **126**, 466 (1993).
[14] Yu. V. Apanovich and E. D. Ljumkis, J. Cryst. Growth **110**, 839 (1991).
[15] O. A. Louchev, S. Otani, and Y. Ishizawa, J. Appl. Phys. **80**, 518 (1996); J. Cryst. Growth (to be published).
[16] A. A. Chernov, in *Modern Crystallography, III* (Springer-Verlag, Berlin, 1984).
[17] O. A. Louchev, J. Cryst. Growth **131**, 209 (1993).
[18] In deriving Eq. (18) we estimated for typical growth rates ($V<10$ cm/h) and diffusion coefficients ($D_1=10^{-8}$–10^{-9} m^2/s) that $\rho_s/\rho_1\ V/D_1 a \ll 1$.
[19] E. Storms and B. Mueller, J. Phys. Chem. **82**, 51 (1978).
[20] S. Otani, T. Tanaka. and Y. Ishizawa, J. Cryst. Growth **100**, 658 (1990).
[21] An additional approximation, i.e., $G_C/a \ll C^0_{\rm eq}(T_i)$, is made since for $\lambda=10^{-6}$–10^{-3} m the value of $G_C/a \cong 10^{24}$–10^{27} m^{-3}, while $C^0_{\rm eq}(T_i)\cong 10^{28}$ m^{-3}.
[22] The relevant radial Biot number given by the ratio of conductive heat transfer resistance R/k to the heat transfer resistance on the lateral surface of the specimen, $1/(h_c+h_r)$, is estimated to be $Bi=0.05-0.17\ll 1$ allowing consideration of the problem in the 1D approximation.
[23] The relevant Peclet number given by the ratio of the convective heat transfer along the specimen pulling direction, $f\rho cR$, to the heat conductance k is estimated $Pe\cong 10^{-3}\ll 1$ allowing the former to be neglected.
[24] O. A. Louchev, J. Cryst. Growth **129**, 179 (1993).
[25] The terms $r/(rM_{\rm B}+M_{\rm La})\, d\rho_{\rm sol}/dT_i$ and $1/(rM_{\rm B}+M_{\rm La})\, d\rho_{\rm sol}/dT_i$ are estimated to be negligibly small in comparison with Eqs. (26) and (26′), respectively.